

# CHEMISTRY

## A European Journal

A Journal of



### Accepted Article

**Title:** From Mesocates to Helicates: Nickel(II) Supramolecular Assemblies Derived from Tetradentate Schiff Bases. Structural, Magnetic and Chiro-Optical Studies.

**Authors:** Albert Escuer, Julia Mayans, Lorenzo Di Bari, Merce Font-Bardia, Lorenzo Arrico, Francesco Zinna, and Gennaro Pescitelli

This manuscript has been accepted after peer review and appears as an Accepted Article online prior to editing, proofing, and formal publication of the final Version of Record (VoR). This work is currently citable by using the Digital Object Identifier (DOI) given below. The VoR will be published online in Early View as soon as possible and may be different to this Accepted Article as a result of editing. Readers should obtain the VoR from the journal website shown below when it is published to ensure accuracy of information. The authors are responsible for the content of this Accepted Article.

**To be cited as:** *Chem. Eur. J.* 10.1002/chem.201800323

**Link to VoR:** <http://dx.doi.org/10.1002/chem.201800323>

Supported by  
**ACES**

WILEY-VCH

# From Mesocates to Helicates: Nickel(II) Supramolecular Assemblies Derived from Tetradentate Schiff Bases. Structural, Magnetic and Chiro-Optical Studies.

Júlia Mayans,<sup>[a]</sup> Mercè Font-Bardia,<sup>[b]</sup> Lorenzo Di Bari,<sup>[c]</sup> Lorenzo Arrico,<sup>[c]</sup> Francesco Zinna,<sup>[c]</sup> Gennaro Pescitelli,<sup>[c]</sup> and Albert Escuer<sup>\*[a]</sup>

**Abstract:** The systematic reactions of a family of tetradentate pyridyl/imine and quinolyl/imine racemic or enantiopure Schiff bases with Ni(NO<sub>3</sub>)<sub>2</sub> or Ni(ClO<sub>4</sub>)<sub>2</sub> in the presence of sodium azide yielded, as a function of the starting racemic, chiral or achiral base, a set of chiral, meso or achiral complexes. In all cases, the compounds consist in two Ni<sup>II</sup> cations linked by a double azido bridge in its end-on coordination mode. All the dimers exhibit a mesocate supramolecular structure and one of them, the unprecedented mix of helicate and mesocate in 2:1 ratio. The transition from mesocate to helicate conformation has been reached tuning the flexibility of the central spacers of the Schiff bases and the size of the substituents. Electronic circular dichroism (ECD) studies have been performed for two pairs of enantiomers and interpreted by means of DFT calculations. Susceptibility measurements show a ferromagnetic coupling between the Ni(II) cations mediated by the end-on azido bridges.

## Introduction

Enantiopure polynuclear transition metal complexes are becoming a subject of great interest in coordination chemistry because they are opening a wide range of possibilities in the synthesis of new materials<sup>[1,2]</sup>, biochemistry,<sup>[3-6]</sup> drug design<sup>[7]</sup> or catalysis.<sup>[8-12]</sup>

Control of chirality in supramolecular structures is a way to relate their properties and reactivity to their structure in a predictive way. It allows the design of complexes with a controlled topology and with specific physical properties as electronic circular dichroism (ECD), circularly polarized luminescence (CPL), non-linear optics, magneto-chiral effects, etc.

Helicates and mesocates built around hexa- or tetra-coordinated metal cations,<sup>[13,14]</sup> are among the most studied supramolecular structures, because the self-assembling between the organic ligands and the metal cations allowed elucidating that the formation of supramolecular structures is directed by parameters as the electronic or steric preferences of the metal, the disposition of the donor atoms in the ligand, or other factors such those postulated by M. Albrecht relating the preference for one or other stereochemistry, for series of ligands with different spacers, with the even or odd number of C-atoms<sup>[15]</sup> of the chain or its flexibility.<sup>[16]</sup>

Ligands must be chosen carefully to prepare compounds of this kind because they must have the ability to link different metal centers in spite of chelating a lonely cation. Bis-bidentate or bis-tridentate ditopic ligands, in which the chelating fragments are linked by a flexible spacer, are extremely useful in this field because they can afford complexes with a great variety of cations. In this sense, the first-row transition metals have been specially studied, although structures with other transition metals or even quadruple helicates with rare earths also appear in the literature.<sup>[17]</sup> Usually, all the coordination sites around the metal are fulfilled by the ligands, resulting in double helicates ([M<sub>2</sub>L<sub>2</sub>]<sup>n+</sup>) when the bis-bidentate ligands react with cations which prefer a tetrahedral environment, or when the bis-tridentate ligands react with cations which prefer an octahedral environment. When pyridyl/imine Schiff bases with ethylene spacer are employed as ligands, systematic characterization of [M<sub>2</sub>L<sub>2</sub>]<sup>n+</sup> helicates have been reported and in both cases, the bidentate or tridentate units around the same cation determine an ideal 90° angle between them. Also in both cases, the torsion angle determined by the NCCN atoms of the flexible spacer lies typically around 60°, as shows the analysis of the 30 reported structures with pyridyl/imine ligands and tetrahedral Cu<sup>I</sup>,<sup>[18-29]</sup> Ag<sup>I</sup>,<sup>[24,25,30-35]</sup> or with bipyridyl/inmine ligands and octahedral Zn<sup>II</sup>, Cu<sup>II</sup> or Fe<sup>III</sup> cations,<sup>[28,36,37]</sup> Scheme 1 (a) and (b). Double Ni<sup>II</sup> helicates with the cations in octahedral environment and with two coordination sites occupied by one bidentate ligand and employing the L2 Schiff base (Scheme 2), exhibit similar coordination sites for the

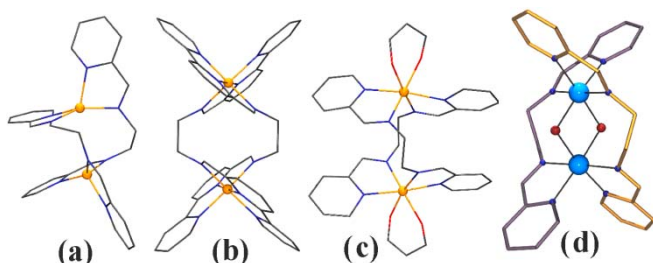
[a] J. Mayans, Prof. A. Escuer  
Departament de Química Inorgànica i Orgànica, Secció Inorgànica  
and Institut de Nanociència i Nanotecnologia (IN<sup>2</sup>UB).  
Universitat de Barcelona  
Martí i Franques 1-11, Barcelona-08028, Spain  
E-mail: [albert.escuer@qi.ub.es](mailto:albert.escuer@qi.ub.es)  
[www.ub.edu/inorgani/recerca/MagMol/magmol.htm](http://www.ub.edu/inorgani/recerca/MagMol/magmol.htm)

[b] Dr. M. Font-Bardia  
Departament de Mineralogia, Cristal·lografia i Dipòsits Minerals and  
Unitat de Difracció de R-X. Centre Científic i Tecnològic (CCiTUB)  
Universitat de Barcelona

[c] Prof. L. Di Bari, Dr. L. Arrico, Dr. F. Zinna, Dr. G. Pescitelli  
Dipartimento di Chimica e Chimica Industriale  
Università di Pisa  
Via Moruzzi 13, I-56124 Pisa, Italy

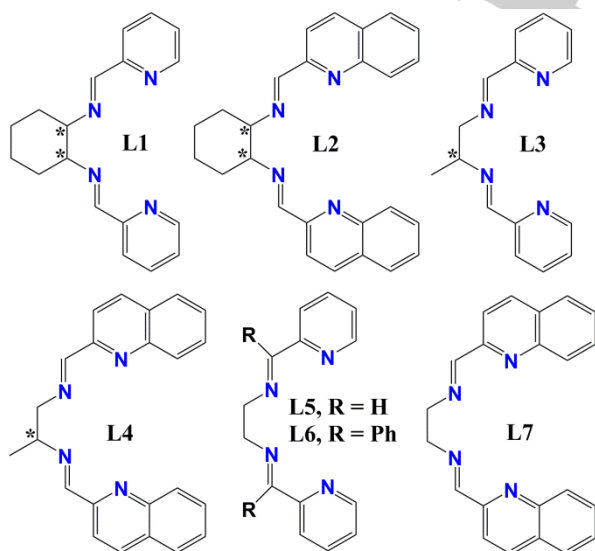
Supporting information for this article is given via a link at the end of the document.

N-donors and NCCN torsion angles in the same range, Scheme 1 (c).<sup>[38]</sup>



**Scheme 1.** Double helicate with bis-bidentate ligands around tetrahedral cations (a), bis tridentate ligands around octahedral cations (b), bis-bidentate ligands around octahedral cations and a bidentate co-ligand (c) and bis-bidentate ligands and two bridging co-ligands around octahedral cations (d).

An special case is provided by double helicates with general formula  $[M_2(L)_2X_2]^{n+}$ , (Scheme 1-d). These systems, in which L corresponds to the bis-bidentate pyridyl/imine Schiff bases L5 or L6 (Scheme 2) and X is a bridging ligand, are scarce and have been only reported for  $Co^{II}$  cations with X = oxo, or peroxy,<sup>[39]</sup> and for  $Ni^{II}$  cations with X = azido or cyanate.<sup>[40]</sup> In all cases the  $[M_2L_2X_2]^{n+}$  dimers exhibit an helicate arrangement and, as a consequence of the relative position of the pyridine ring, the corresponding NCCN torsion angle of the spacer becomes much larger, typically in the 80°-90° range. An interesting characteristic of this kind of structures is that in contrast with the  $\Lambda\Delta$  mesocates, the helicity implies homochiral ( $\Lambda\Lambda$  or  $\Delta\Delta$ ) stereochemistry around the metallic centers.



**Scheme 2.** Ligands employed (L1, L2, L3, L4, L7) or referenced (L5, L6) in the present work. Asterisks denote the chiral C-atoms for ligands L1 to L4.

With the aim to characterize new  $[M_2L_2X_2]^{n+}$  complexes and to study the relationship between helicates and mesocates in this kind of systems that requires unusual NCCN torsion angles, we choose for this work a family of bis-bidentate Schiff bases (Scheme 2), containing four N-donor nitrogen atoms with a NCCN spacer able to promote the formation of discrete metal-ligand complexes. Three aspects have been taken into account to understand better the self-assembling of these structures. First, the tuning of the flexibility of the central saturated C-C bond of the spacer permits to study its influence in the final product: when the C-C bond presents a high degree of flexibility, the helicate structure should be allowed while for a low degree of flexibility, only the mesocate should be achieved. Second, the steric effect of the aromatic substituents in the ligand was varied to check its influence in the final conformation and third, the effect of the chirality was considered as a driving force to get helicates against the former effects, because of as can be found in the literature,<sup>[41,42]</sup> when an organic ligand with a stereogenic center is used, it usually tends to yield chiral supramolecular helicate structures with the same configuration  $\Lambda\Lambda$  or  $\Delta\Delta$  for all the octahedral metal centers.

In this work we report the syntheses and characterization of a series of complexes with general formula  $[Ni_2L_2(N_3)_2]A_2$  (A =  $NO_3^-$ ,  $ClO_4^-$ ), obtained by the reaction of the corresponding  $NiA_2$  salt with the selected L Schiff base in the presence of sodium azide, resulting in various kinds of compounds: the meso **1M** and the chiral (**1SS**, **1RR**) mesocate complexes with general formula  $[Ni_2(L1)_2(N_3)_2](NO_3)_2$ ; the chiral mesocates  $[Ni_2(L2)_2(N_3)_2](NO_3)_2$  (**2SS**, **2RR**); several derivatives of L3 (**3**) with A =  $NO_3^-$  or  $ClO_4^-$  for which the structure was not fully determined; the mesocate  $[Ni_2(R-L4)_2(N_3)_2](ClO_4)_2$  (**4R**); and the rare mixing in 1:2 ratio of mesocate and helicate conformations derived from the achiral ligand L7 with formula  $[Ni_2(L7)_2(N_3)_2](NO_3)_2$  (**7**).

All the synthesized complexes are dinuclear structures, as was expected, and they join several unusual features: the transition from mesocate to helicate has been tuned by changes in the ligands, showing in one case the unprecedented coexistence of mesocates and helicates in the same network; moreover, we achieved the synthesis of rare chiral mesocates due to the chirality of the ligands. In addition to the structural study, the systems have been characterized by electronic circular dichroism (ECD), DFT calculations and magnetic susceptibility measurements

## Results and Discussion

### Description of the structures

The structures of the reported complexes are similar in their general trends. To avoid repetitive descriptions, the structure of **1M** will be described in detail and only the more important features will be discussed for the remainder complexes. Intermolecular interactions and the supramolecular arrangement in the network will be discussed separately.

**meso-[Ni<sub>2</sub>(L1)<sub>2</sub>(N<sub>3</sub>)<sub>2</sub>](NO<sub>3</sub>)<sub>2</sub>·2MeOH (1M·2MeOH).** The molecular structure of **1M** consist of a centrosymmetric cationic Ni<sup>II</sup><sub>2</sub> complex (Figure 1) and two NO<sub>3</sub><sup>-</sup> counteranions. The main bond parameters are summarized in Table S1. Each bidentate pocket of the L1 ligand is coordinated to a different Ni<sup>II</sup> cation, acting as a bis-bidentate ligand. The Ni<sup>II</sup> cations are octahedrally coordinated in a *cis* fashion by two bidentate fragments of L1 and two azido ligands in its end-on coordination mode. The main distortion of the octahedron is due to the low bit angle of the bidentate fragments that gives N<sub>imine</sub>-Ni-N<sub>py</sub> bond angles around 80°. The Ni<sub>2</sub>N<sub>2</sub> (Ni-(N<sub>azido</sub>)<sub>2</sub>-Ni) central ring is planar with similar distances to the azide bridging atoms, 2.104(1)-2.099(1) Å, with a Ni···Ni distance of 3.0339(3) Å. The azido ligands form an angle of 42.8(2)° with the mean Ni<sub>2</sub>N<sub>2</sub> plane. The hexane ring shows a chair conformation, with a N(2)-C(7)-C(12)-N(3) torsion angle of 54.5(3)°. Each L1 ligand possesses two chiral C-atoms related by the inversion center placed in the dinuclear unit, and thus one possesses *RR* and the other *SS* chirality. In this complex, the L1 ligands are surrounding the Ni<sup>II</sup> cations in a mesocate arrangement and consequently, the two Ni<sup>II</sup> cations exhibit opposite  $\Lambda$  /  $\Delta$  stereochemistry. The pyridyl rings linked to the same Ni<sup>II</sup> cation form a 97.8° angle between mean planes. Intermolecular interactions between dinuclear units are weak CH···N and CH···O H-bonds involving the nitrate counteranions, methanol solvent molecules and terminal N-atoms of the azido ligands and the only stronger OH···O H-bonds present in the network are those between the methanol molecules and the nitrate counterions.

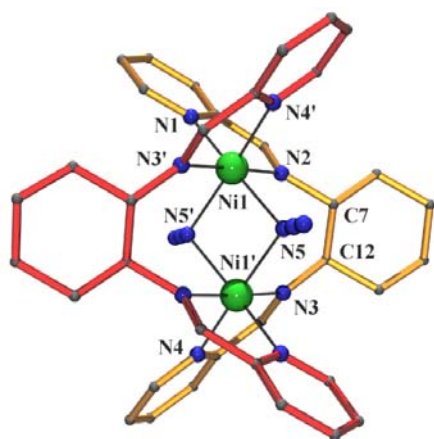


**Figure 1.** Partially labelled view of the mesocate cationic dinuclear complex **1M**. Colour key for all figures: Ni<sup>II</sup>, green; N, navy blue; C, dark grey.

**[Ni<sub>2</sub>(RR-L1)<sub>2</sub>(N<sub>3</sub>)<sub>2</sub>](NO<sub>3</sub>)<sub>2</sub>·2MeOH (1RR·2MeOH) and [Ni<sub>2</sub>(SS-L1)<sub>2</sub>(N<sub>3</sub>)<sub>2</sub>](NO<sub>3</sub>)<sub>2</sub>·2MeOH (1SS·2MeOH).** The structures of both enantiomers are practically identical and thus the following description is centered on **1RR**, shown in Figure 2. Selected bond angles and distances for **1RR** are listed in Table S2. As the above described **1M** complex, the dimers show a mesocate arrangement but in this case the dimers are not centrosymmetric.

Ni-N<sub>azide</sub>-Ni bond angles are quasi identical (92.1°/92.5°) with an angle between the azides and the main Ni<sub>2</sub>N<sub>2</sub> plane of 43.5°. The octahedral coordination sphere of Ni(1) consists of two bonds to the bridging azido ligands, two N<sub>imine</sub> and two N<sub>py</sub> donors with Ni-N bond distances clearly larger for Ni-N<sub>imine</sub> than for Ni-N<sub>py</sub>. The situation is reversed around Ni2, which shows Ni-N<sub>imine</sub> bond distances shorter than the Ni-N<sub>py</sub> bond distances. The NCCN torsion angles of the central spacer (44.9(3)° / 49.0(3)°) are lower than for **1M**. As consequence of these differences, the angle between pyridine rings linked to the same Ni<sup>II</sup> cation is also asymmetric with values of 92.4(2)° for the rings linked to Ni1 and 103.8(2)° for the pyridine rings linked to Ni2. The intermolecular interactions are similar to **1M**.

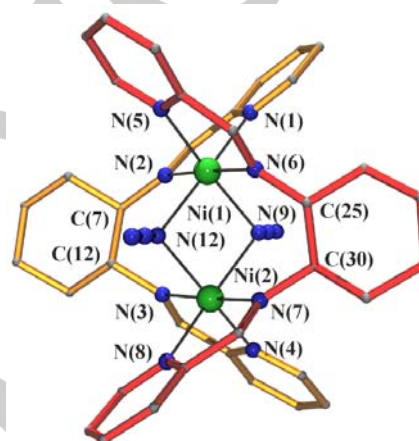


**Figure 2.** Partially labelled plot of complex **1RR**. Atom labels are common for **1RR** and **1SS**.

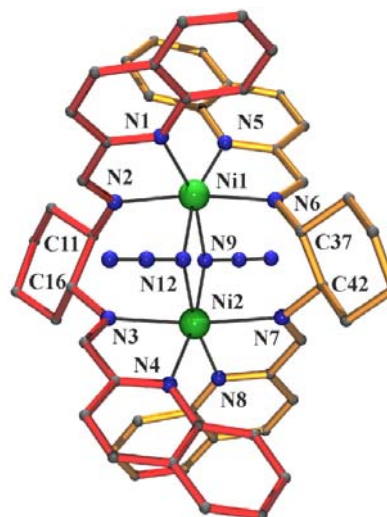


**Figure 3.** Partially labelled plot of complex **2SS**, common with **2RR**.

**[Ni<sub>2</sub>(RR-L2)<sub>2</sub>(N<sub>3</sub>)<sub>2</sub>](NO<sub>3</sub>)<sub>2</sub>·3MeOH (2RR·3MeOH) and [Ni<sub>2</sub>(SS-L2)<sub>2</sub>(N<sub>3</sub>)<sub>2</sub>](NO<sub>3</sub>)<sub>2</sub>·3MeOH (2SS·3MeOH).** The mesocate structures of **2RR** and **2SS** are similar in their general trends to the above described complexes **1RR** and **1SS**. In the case of **2RR** and **2SS** there are two similar but nonequivalent dimers in the unit cells, labelled A and B. Selected bond parameters are listed in Table S3 and a view of the A unit of **2RR** is shown in Figure 3. The coordination spheres of Ni(1) and Ni(2) are also different, being the Ni-N<sub>imine</sub> bond distances clearly shorter than the Ni-N<sub>py</sub> for Ni(1) (mean values 2.059 and 2.120 Å respectively), whereas the situation is opposite for Ni(2), with Ni-N<sub>imine</sub> mean bond distance of 2.179 Å and Ni-N<sub>py</sub> of 2.124 Å. The NCCN torsion angles take values of 48.1(7)°/47.6(6)° for molecule **2RR-A** and 52.8(6)°/51.3(6)° for molecule **2RR-B**, and the angles between the quinoyl mean planes linked to the same Ni<sup>II</sup> cations are clearly different with values of 110.5(2)°/106.3(2)° for the A unit and 94.2(2)°/91.0(2)° for the B unit and Ni1 / Ni2, respectively.

**[Ni<sub>2</sub>(R-L4)<sub>2</sub>(N<sub>3</sub>)<sub>2</sub>](ClO<sub>4</sub>)<sub>2</sub>·xMeOH (4R·xMeOH)**

A labeled plot of **4R** is shown in Figure 4 and the main bond parameters are listed in Table S4. The molecular structure of the mesocate complex **4R** is very similar to the above described complexes **2RR/SS** with two independent dimers (labeled as A or B) in the unit cell, similar Ni-N-Ni bond angles and the same Ni-N<sub>imine</sub> / Ni-N<sub>qx</sub> bond distances relationship for Ni1 and Ni2. The main differences lie in the lower NCCN torsion bonds with values of 48.3(9)°/39.3(9)° for the A unit and 39.1(7)°/33.9(8)° for the B dimer. The dihedral angle between mean quinoyl planes linked to the same Ni<sup>II</sup> cation is similar in both dimers ranging between 104.9(3)° and 109.9(2)°.

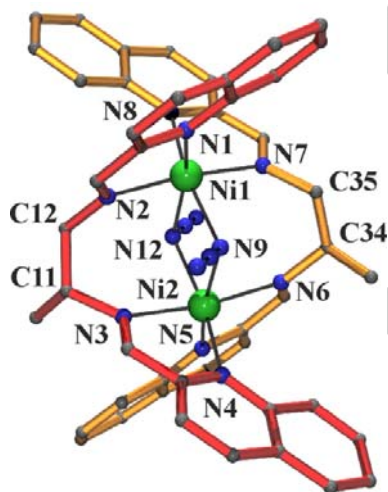


Figure 4. Partially labelled plot of complex **4R**.

**[Ni<sub>2</sub>(L7)<sub>2</sub>(N<sub>3</sub>)<sub>2</sub>](NO<sub>3</sub>)<sub>2</sub>·2H<sub>2</sub>O·2MeOH (**7**)**

The exceptional structure of compound **7** consists of two non-equivalent dimers labeled A and B, one of them with mesocate centrosymmetric arrangement (**7B**) and the other with helicate

non-centrosymmetric structure (**7A**). The presence of inversion centers in the network generates two molecules with opposite helicity **7A-Δ** and **7A-Λ** and thus, there are three different dimers in the achiral network. The main bond parameters are listed in Table S5 and a view of the mesocate and one of the helicates is shown in Figure 5. The mesocate unit **7B** is similar to the previously described systems with the same conformation, showing larger Ni-N<sub>qx</sub> bond distances than the Ni-N<sub>imine</sub> ones, a NCCN torsion of the central spacer of 50.1(7)°, and a dihedral angle between quinoyl mean planes of 94.0(1)°.

The **7A** helicate molecule shows Ni-N<sub>qx</sub> > Ni-N<sub>imine</sub> bond distances for both Ni1 and Ni2 environments and similar dihedral angle between the quinoyl planes (110.8(2)° / 108.0(2)°). The key difference with the precedent mesocates lies, as expected, in the larger NCCN torsion angles that take values of 83.7(6)° and 81.2(5)°. Ni-N-Ni bond angles are 99.3(2)° and 100.5(2)°.

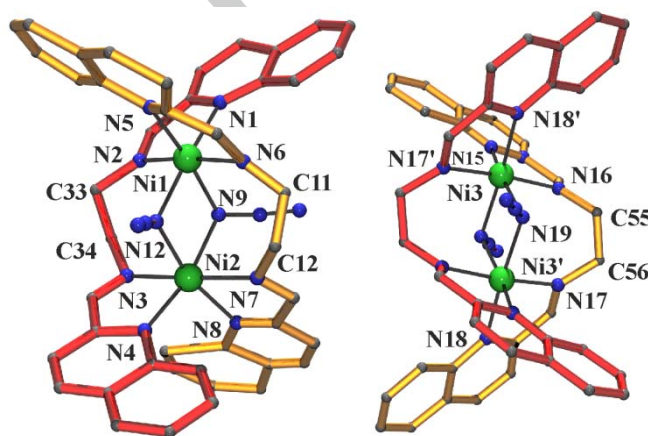


Figure 5. Partially labelled plot of the helicate **7A** (left) and the mesocate **7B** (right) complexes.

**[Ni<sub>2</sub>(L3)<sub>2</sub>(N<sub>3</sub>)<sub>2</sub>]<sub>2</sub>A<sub>2</sub>·solvent (A = NO<sub>3</sub><sup>-</sup>, ClO<sub>4</sub><sup>-</sup>) (**3**)**

Diffraction data were collected for multiple crystals of the complexes derived from *rac*-L3 or chiral-L3 ligand and nitrate or perchlorate counteranions but the trials to solve the structure were unsuccessful. The complexes crystallize in nice polyhedral crystals that diffract correctly but fails in the refinement process. The obtained molecules show images in which both conformations seems overlapped and with disordered azido ligands with large deviation from linearity, Figure S1. In light of the partial structural results, the presence of both mesocate and helicate conformations, even must be assumed with caution, seems to be consistent.

**Network supramolecular arrangement.**

The most conventional non-covalent interaction forces that determine the network supramolecular arrangement for systems containing aromatic rings are typically the π-π stacking. In addition and equally important, electron-deficient aromatic rings

like those containing coordinated N-donors can promote other interactions that revealed determinant in biological systems, but rarely studied in cluster chemistry, such anion- $\pi$  or lone pair- $\pi$  interactions.<sup>[43]</sup> Also, the weaker  $\text{CH}\cdots\pi$  interaction revealed as determinant in the crystal packing.<sup>[44]</sup> Complexes **1M**, **1RR** and **1SS** containing pyridyl rings do not show remarkable interdimer interactions in the network. In contrast, when the quinolyl aromatic fragment is present in the structures, it promotes intermolecular interactions which determine the spatial arrangement of the molecules. Intermolecular interactions in complexes **2RR** and **2SS** are dominated by the  $\pi$ - $\pi$  stacking of the aromatic rings of the quinolyl groups, which show a distance between the centroids of the phenyl fragments of 3.645 Å. In addition, there are two  $\text{CH}\cdots\pi$  interactions between one of the H-atoms of the phenyl ring and one phenyl fragment of the neighbor molecule (H-centroid distances of 2.565 and 3.152 Å). As a consequence of these interactions, the molecules are ordered forming parallel chains where the A and B nonequivalent dimers present in the unit cell are arranged in ABABA alternance along the chains, Figure 6.

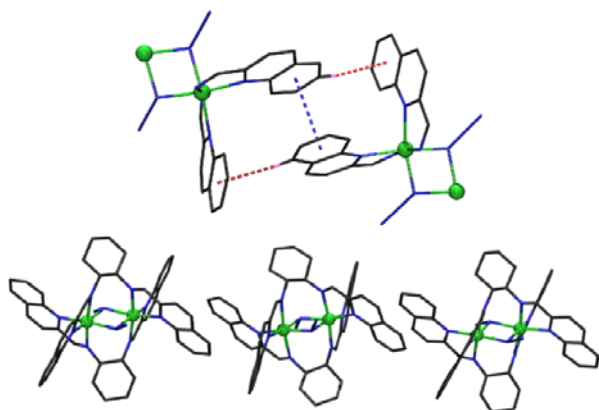


**Figure 6.** Top, intermolecular interactions found in compounds **2RR** and **2SS**.  $\pi$ - $\pi$  stacking is indicated as blue dotted lines between centroids and H-ring contacts as red dotted lines. Bottom, lateral view of the 1-D arrangement of the dimers.

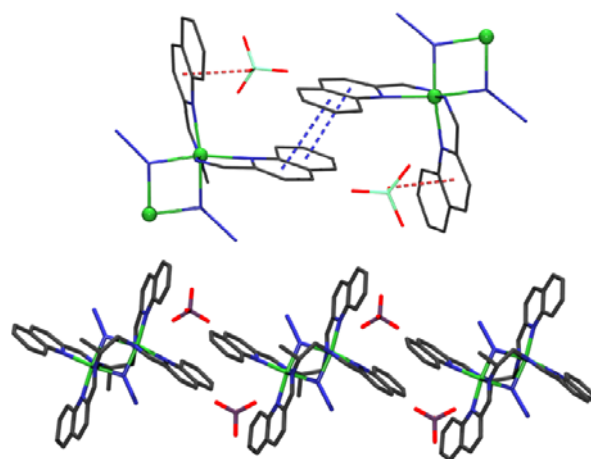


**Figure 7.** Top, intermolecular interactions found in compound **4R**.  $\pi$ - $\pi$  stacking is indicated as blue dotted lines between centroids and O-ring contacts as red dotted lines. Bottom, lateral view of the 1-D arrangement of dimers.

As in the previous case, the structure of **4R** contains two non-equivalent dimers (named A and B). The network consists in layers of parallel chains of B molecules and non-interacting A dimers between the layers, which are surrounded by perchlorate anions and solvent molecules giving a complicated set of weak  $\text{C-H}\cdots\text{O}$  H-bonds. The interaction that generates the B chains is the  $\pi$ - $\pi$  stacking of the quinolyl fragments with interplanar distance of around 3.3 Å, and a distance between the centroids of the phenyl and the pyridyl fragments of 3.542 Å. In this case, one O-atom of the perchlorate counteranion gives an anion- $\pi$  ring interaction with a distance between the O-donor and the centroid of the pyridyl ring of 2.900 Å. This interaction avoids the possibility of  $\text{CH}\cdots\pi$  interactions, Figure 7.

The structure of complex **7** contains a centrosymmetric mesocate and two helicates with opposite  $\Delta / \Lambda$  helicity. The intermolecular interactions provide an exceptional example of chiral recognition in an achiral network. The mesocates form layers of parallel chains of dimers linked by the same kind of intermolecular interactions as have above described for compounds **2RR/2SS** Figure 6, namely,  $\pi$ - $\pi$  stacking of the aromatic rings of the quinolyl groups, with a distance of 3.424 Å between main planes and of 3.715 Å between centroids, plus symmetric  $\text{CH}\cdots\pi$  ring interactions (H-centroid of the phenyl ring distance of 2.866 Å). Between the mesocate planes there are layers of helicates formed by homochiral parallel chains of  $\Lambda\Lambda$  and  $\Delta\Delta$  dimers related by inversion centers, Figure 8. In these helical chains the intermolecular interactions are dominated by double  $\text{CH}\cdots\pi$  ring interactions with H-ring(pyridyl) distance to centroids of 2.643 Å and H-ring(phenyl) of 2.901 Å, respectively. The  $\pi$ - $\pi$  stacking is less effective than for the mesocates because the aromatic rings are not parallel.

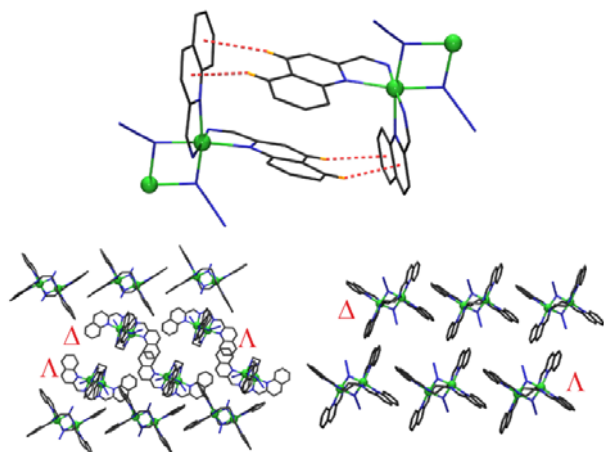


**Figure 8.** Top, intermolecular interactions found in compound **7A-Δ** and **7A-Δ**.  $\text{CH}\cdots\pi$  ring contacts are indicated as red dotted lines. Bottom (left), one layer of chains of  $\Delta$  and  $\Lambda$  dimers between layers of parallel chains of mesocates. Bottom (right), a lateral view of the parallel  $\Delta$  and  $\Lambda$  chains of helical dimers.

### Electronic and Vibrational Circular Dichroism.

Vibrational circular dichroism (VCD) of **1RR/SS** and **2RR/SS** in the solid state (KCl pellets) was preliminarily investigated, in search of metal-induced VCD enhancements.<sup>[45,46]</sup> However, no VCD enhancement was observed, probably because there are no  $d-d$  transitions of suitable energy to effectively mix with the vibrational transitions.<sup>[47]</sup> In these conditions, the VCD signals are too weak with respect to the artifacts due to linear anisotropies in the solid state; therefore, it was not possible to obtain reliable VCD spectra.

Solid-state ECD spectra were measured as KCl pellets for **1RR** and **1SS** in the 350-900 nm region. They display several bands with non-negligible rotational strength (Figure 9, top). These bands have an expected main  $d-d$  character; however, their nature is in fact more complex (see the computational analysis section). The spectra measured on the two enantiomers are perfectly mirror images, ensuring that there are no significant contributions from linear dichroism/linear birefringence.<sup>[48]</sup> In this case it was not possible to obtain a disc of sufficient quality to penetrate below 350 nm. Solution spectra measured in acetonitrile display several and relatively intense bands also in the 200-350 nm region, where the character of the transitions is mainly – although not exclusively – ligand-centered (Figure 9, bottom).

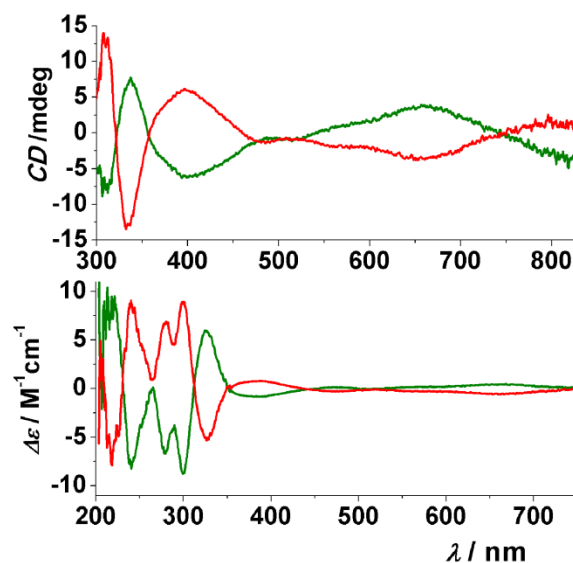


**Figure 9.** Top, solid state ECD spectra recorded for the **1RR** (green line) and **1SS** (red line) enantiomers. The spectra were recorded on KCl pellets. Bottom, normalized solution ECD spectra in  $\text{CH}_3\text{CN}$  recorded for **1RR** and **1SS** enantiomers. The spectra were recorded using a 0.1 cm cell for the 200-380 nm region and a 1 cm cell for the 380-900 nm region.

For complexes **2RR/SS** it was possible to obtain KCl discs suitable to penetrate down to 250 nm (Figure 10, top). We notice that the intensity ratio between long-wavelength and short-wavelength transitions is lower than in the **1RR/SS** case. This fact is appreciable both in the solid state and in solution spectra (Figure 10, bottom), and is related to the stronger electronic transitions of the quinoline chromophores with respect to the pyridine ones.

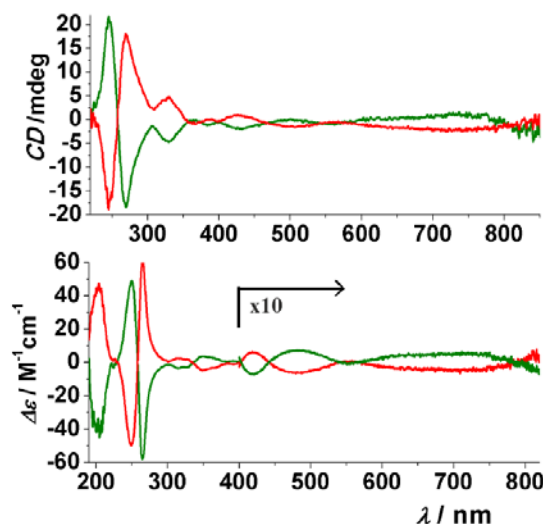


**Figure 10.** Top, solid state ECD spectra recorded for the two **2RR** (green line) and **2SS** (red line) enantiomers. The spectra were recorded on KCl pellets. Bottom, normalized solution ECD spectra in  $\text{CH}_3\text{CN}$  recorded for **2RR** and **2SS** enantiomers. The spectra were recorded using a 0.1 cm cell for the 200-380 nm region and a 1 cm cell for the 380-900 nm region.

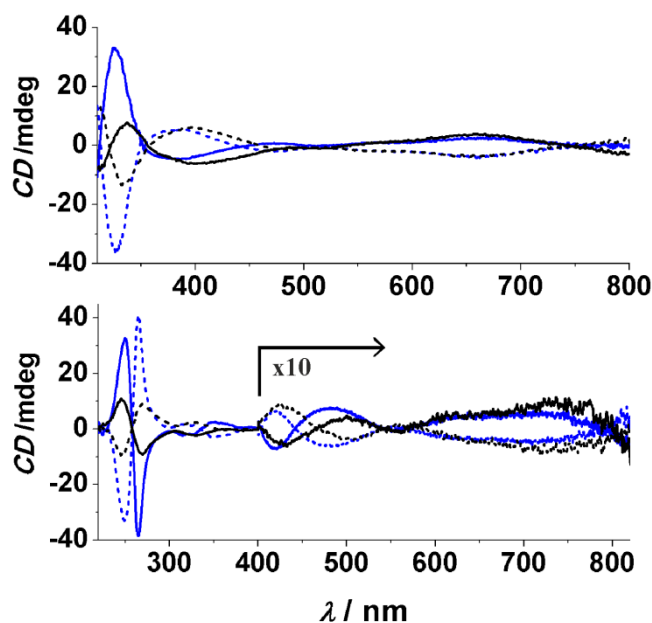


**Figure 11.** Comparison between solid state (blue lines) and solution (black lines) ECD spectra for **1RR** and **1SS** (top) and for **2RR** and **2SS** (bottom). *RR* enantiomers, continuous lines; *SS* enantiomers, dotted lines.

It is interesting to compare the solution and the solid-state ECD spectra. It is apparent from Figure 11 that the two pairs of spectra are almost perfectly superimposable in the longer wavelength region, 400–900 nm, while shorter wavelength transitions (above 350 nm) maintain the same shape and sign in the two media but with different relative intensity; a higher intensity is observed in solution than in the solid state. This indicates that, although small ligand rearrangements can occur upon solvation, Ni-centered transitions are not significantly affected. Furthermore, intermolecular interactions which may occur in the microcrystalline solid-state samples are more effective for ligand-centered transitions, because of their stronger electric-dipole allowed character.<sup>[49]</sup>

Time-dependent density functional theory (TDDFT) was employed to simulate the ECD spectra of compounds **1SS**.<sup>[50]</sup> It must be stressed that excited-state calculations of open-shell Ni complexes with high spin are very demanding.<sup>[51,52]</sup> In the current case the situation is further complicated by the presence of four chromophores each with several transitions. In fact, a very high number of transitions needed to be considered, however, TDDFT calculations are intrinsically less accurate for high-lying states.<sup>[53]</sup> As a consequence, only a portion of the ECD/UV spectra may be investigated (above  $\approx 300$  nm), and our analysis is not expected to perfectly reproduce the experimental spectra. In Figure 12 we show the absorption and CD spectra calculated for **1SS** at CAM-B3LYP/LanL2DZ level, which gave the best results (see Computational Section). The input structure was obtained by reoptimizing the X-ray geometry with DFT at the

B3LYP/6-31G(d) level of theory; an input structure with +2 charge (devoid of counteranions) and quintet spin state was used in all calculations.

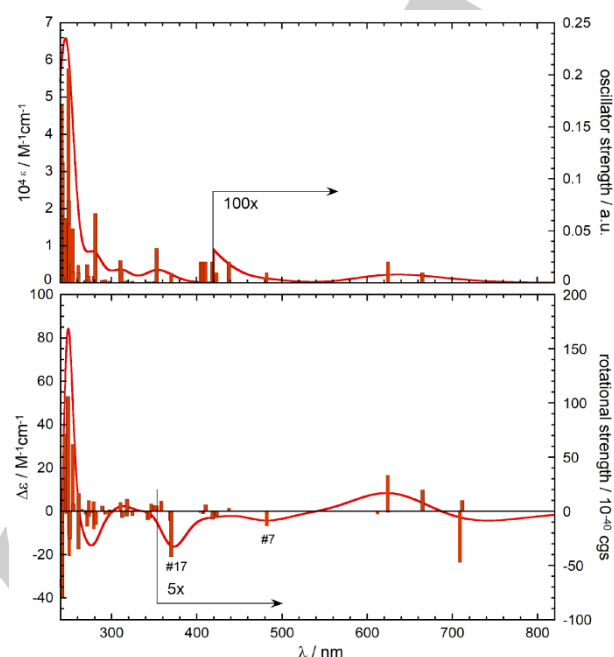


**Figure 12.** TDDFT calculated absorption (top) and ECD (bottom) spectra for compound **1SS** at CAM-B3LYP/LanL2DZ level. Vertical bars represent calculated transitions with respective rotational and oscillator strengths. Spectra were plotted as sums of Gaussian with exponential band-width of 0.3 eV.

Many distinct transitions contribute to the observed absorption and ECD bands; moreover, orbital and population analysis reveal that each transition is due to several different single excitations. This renders a full spectrum assignment impossible in terms of easily identified transitions, especially because there is no clear separation between metal- and ligand-centered transitions, and metal-centered transitions occur deeply in the UV region of the spectrum. We have already observed this behavior before for high-spin Ni complexes with chromophoric ligands.<sup>[52]</sup> As an example, we summarize the assignment of the two transitions most contributing to the two observed negative ECD bands observed around 650 and 480 nm of **1SS**, calculated at 482 (transition labelled #7 in Figure 12) and 370 nm (#17), respectively. The former band is a mixing of several excitations, the dominant ones being those from the  $\pi_{C=N}$ ,  $\pi_{py-C=N}$  and  $d_{xz}$  orbitals to a mixed  $\pi_{N3}^*+d_{yz}$  orbital, respectively (the z axis is along the Ni-Ni direction). The latter band is also a mixing of many excitations, the dominant ones being those from a mixed the  $\pi_{py-C=N}+d_{y2+z2}$  orbital to the two mixed  $\pi_{py}^*/d_{yz}$  and  $\pi_{py}^*/d_{x2}$  orbitals. One clear result from the calculations is that the apparent baseline drift above 800 nm in the ECD spectra is due to a real ECD band, and possibly a further ECD signal with opposite sign is present at even longer wavelengths.

#### Helicate vs mesocate conformation

Helicates and mesocates are supramolecular structures formed by the self-assembly of metallic centers and bridging ligands, as has been told previously. Double helicates with  $M_2L_2$  and triple helicates with  $M_2L_3$  stoichiometry are formed by bis-bidentate ligands bound to two tetrahedral or octahedral metal centers, respectively. In the latter case, this arrangement generates a homochiral ( $\Lambda\Lambda$  or  $\Delta\Delta$ ) helical structure. For a dinuclear double helix built with this type of ligands, it is postulated that the spacer must have an adequate size, enough rigidity to sterically favor the coordination of the two bidentate fragments to different cations, and it also needs enough flexibility to permit the wrap around the  $M \cdots M$  axis of the molecule.

For cations showing octahedral coordination, the triple  $M_2L_3$  helicates with  $C_3$  symmetry are the most common structures Figure 13, left. In this case, the main axis of the molecule is placed on the center of opposite triangular faces of the octahedra and NCCN torsions around  $60^\circ$  are enough to satisfy the helicate requirements. A large number of  $M_2L_2$  ( $M = \text{tetrahedral Cu}^I, \text{Cu}^{II}, \text{Ag}^I$ ) helicates have been reported for ligands with a two-C spacer like the ones employed in the present work, with NCCN torsion angles also around  $60^\circ$ .<sup>[18-35]</sup> In contrast, for the less common  $ML_2X_2$  double helicates with monoatomic or small double  $M-X-M$  bridges, the symmetry is reduced to  $C_2$  with the main molecular axis along the center of opposite edges of the octahedra, Figure 13, right.

This arrangement requires larger NCCN torsion angles closer to  $90^\circ$ , as it has been experimentally proved for  $[\text{Ni}_2(\text{L}5)_2(\mu_{11}\text{-N}_3)_2](\text{ClO}_4)_2$  (NCCN =  $78(1)^\circ/80.0(9)^\circ$ ),  $[\text{Ni}_2(\text{L}6)_2(\mu_{11}\text{-N}_3)_2](\text{ClO}_4)_2$  (NCCN =  $92.8(4)^\circ/93.4(4)^\circ$ ),  $[\text{Ni}_2(\text{L}6)_2(\mu_{11}\text{-NCO})_2](\text{ClO}_4)_2$  (NCCN =  $93.8(4)^\circ/94.0(4)^\circ$ ),<sup>[38]</sup>  $[\text{Co}_2(\text{L}5)_2(\mu\text{-O})(\mu\text{-O}_2)]\text{A}_2$  ( $\text{A} = \text{BF}_4^-$ , NCCN =  $80.2(5)^\circ/81.1(5)^\circ$ ;  $\text{A} = \text{ClO}_4^-$ , NCCN =  $80.5(3)^\circ/81.1(3)^\circ$ ).<sup>[39,40]</sup>

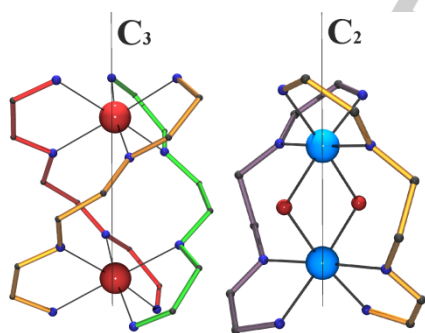


**Figure 13.** Main axial symmetry for triple  $M_2L_3$  (lower NCCN torsion) and  $ML_2X_2$  double helicates (larger NCCN torsion).

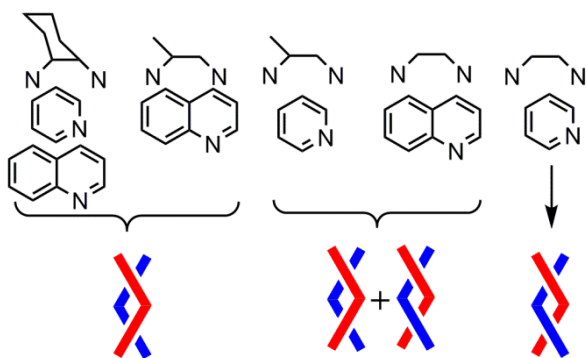
In light of these data, our aim was to explore the reactivity of ligands with different flexibility or aromatic donors with different size in order to tune the selective syntheses of homochiral ( $\Lambda\Lambda$  or  $\Delta\Delta$ ) helicate or heterochiral ( $\Lambda\Delta$ ) mesocate structures for the  $ML_2X_2$  case and to obtain experimental evidence of the factors that determine the formation of one or another type of structure. Steric requirements were centered on the flexibility of the C-C central spacer and size of the aromatic rings. Our starting point was the analysis of the experimentally reported torsion angles

on the C-C=NCCN=C-C fragment belonging to any kind of Schiff bases for the spacers cyclohexane (690 structures), Me-ethyl (72 structures) and ethyl (2865 structures). From these data emerge two interesting features: first, the preferred NCCN torsion angle of the spacer lies around  $40^\circ\text{-}50^\circ$  with practically a 50% of the structures falling in this range and second, the ethyl fragment appears to be more flexible than the cyclohexane or methylethyl fragments, showing several structures with NCCN torsion angles larger than  $80^\circ$  (Figure S2). The same analysis for the pyridyl ligands L1 (46 structures), L3 (9 structures) and L5 (95 structures) reflect the same general trends, that is to say, the same preferred torsion angle and the larger flexibility of the ethyl fragment: for L1 in all cases the NCCN torsion is comprised between  $39.5^\circ$  and  $73.8^\circ$  with one unique case reaching  $78^\circ$ ; for L3 the torsion lies in the very short range of  $45.2^\circ\text{-}66.6^\circ$ ; whereas, for L5 it spans all values between  $0^\circ$  and  $93.8^\circ$ , Figure S3. There are a few reported complexes for the quinoyl ligands L2 (12 structures), L4 (zero structures) and L7 (3 structures), and even if the available information is scarce, it indicates that the NCCN torsion for L1 is limited to a short range of angles comprised between  $53\text{-}66^\circ$ . From this structural analysis, the larger flexibility of the ligand for unsubstituted spacers and smaller ring size can be inferred.

As could be expected, the most rigid ligand are those containing the cyclohexane ring that prevents extreme torsions and effectively, L1 and L2 are not enough flexible in the spacer to produce the helicate. As a experimental confirmation, the mesocate arrangement was obtained for **1M**, **1SS**, **1RR**, **2SS** and **2RR**.

L3 and L4 should be in principle slightly more flexible in the spacer than their analogous L1 and L2 with cyclohexane spacer and, according to the previous analysis, L3 should be more flexible than L4. Then, is not surprising that the mesocate arrangement is the preferred form for **4R**, whereas both helicate and mesocate forms seems to be equally preferred for L3. In the same way and following the same tendencies, both forms seem to be equally favored for the quinoyl ligand L7 with an ethyl spacer, whereas the helicate is exclusively formed for the previously reported<sup>[38-40]</sup> most flexible ligands L5 and L6.

Thus, we can conclude that the combination of the flexibility of the spacer and the difference in the volume of the aromatic chromophore, promotes a well-established effect on the resulting supramolecular arrangement, showing a perfect transition from mesocate to helicate arrangement for the  $ML_2(\mu\text{-X})_2$  case. The combination of both effects can be graphically seen in Scheme 3.



**Scheme 3.** Helicite to mesocate transition as function of the spacer and ring size of the Schiff bases.

On the other hand, the transfer of chirality from the chiral center of the ligands to the cations or the whole supramolecular assembly is a common fact and it is widely accepted that chiral molecules (ligands in the particular case of coordination chemistry) generate chiral supramolecular systems. This interesting feature, where the ligand transfers its chirality to the metal centers, has been called predetermined chirality<sup>[9,41,42]</sup> being the  $\Lambda\Lambda$  or  $\Delta\Delta$  configurations of the stereogenic metal centers completely controlled by the chiral configuration of the ligands.<sup>[54]</sup> In our case, this assumption means that the employment of enantiomerically pure ligands should lead to the formation of homochiral helicates with homochirality at level of the metal centers and helicity of the molecules. However, in contrast with these rules, for compounds **1SS**, **1RR**, **2SS**, **2RR** and **4R** for which chiral ligands were employed, the mesocate configuration was obtained. These results highlight the possibility that even when the ligand has a stereo definite chiral center and the bridging mode of the ligand allows for conformational chirality, the final structure cannot present an overall chirality by rational control of the properties of the ligand. On the other hand, the final mesocates retain the chirality only through the presence of asymmetric C-atoms of the ligands, resulting in the extremely unusual chiral mesocates.

### Susceptibility studies

The magnetic response for double azido bridges with Ni-N-Ni bond angles has been well established, giving strong ferromagnetic interaction for bond angles around  $100^\circ$ .<sup>[55]</sup> To check the magnetic properties of the reported compounds, susceptibility measurements were performed for the series of compounds **1** and **2**. **1M**, **1RR** and **1SS** show quasi identical plots, as does the pair of **2RR** and **2SS** isomers. Therefore, only one measurement for each family of enantiomers will be discussed. Room temperature  $\chi_M T$  value for compound **1RR** is  $2.62 \text{ cm}^3 \text{ mol}^{-1} \text{ K}$ , larger than the expected value for two isolated  $S = 1$  centers ( $2.0 \text{ cm}^3 \text{ mol}^{-1} \text{ K}$  for  $g = 2.00$ ). Upon cooling, the  $\chi_M T$  product increases gradually up to 16 K ( $3.56 \text{ cm}^3 \text{ mol}^{-1} \text{ K}$ ). Below this temperature, the  $\chi_M T$  product decreases down to  $3.15 \text{ cm}^3 \text{ mol}^{-1} \text{ K}$  at 2 K, Figure 14. Complex **2RR** has a similar response with room temperature  $\chi_M T$  value of  $2.77 \text{ cm}^3 \text{ mol}^{-1} \text{ K}$ , a

maximum value of  $3.56 \text{ cm}^3 \text{ mol}^{-1} \text{ K}$  at 20 K and a final value of  $3.23 \text{ cm}^3 \text{ mol}^{-1} \text{ K}$  at 2 K. The  $\chi_M T$  plots evidence strong intramolecular ferromagnetic interactions between the  $\text{Ni}^{\text{II}}$  centers. Considering the structural data that do not show relevant intercluster interactions, the decay of  $\chi_M T$  at low temperature should be attributed to  $D$  effects.

A fit of the experimental data was performed in the full range of temperature with PHI program<sup>[56]</sup> on basis of the Hamiltonian  $H = -2J_1(S_1 \cdot S_2)$  and including a  $D_{\text{ion}}$  term.

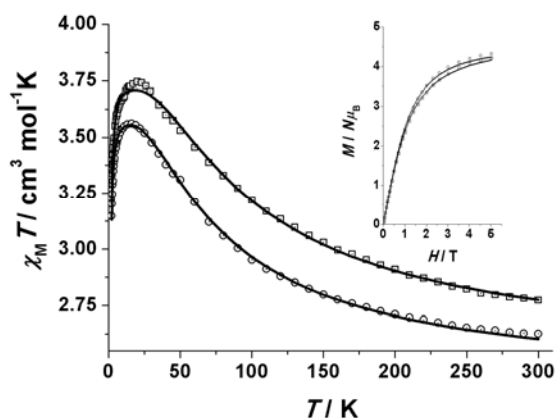


**Figure 14.** Plot of the  $\chi_M T$  product vs.  $T$  for compounds **1RR** (circles) and **2RR** (squares). Inset, magnetization plots. Solid lines show the best fits of the experimental data.

The best fit of the experimental data gave  $J = +14.9 \text{ cm}^{-1}$ ,  $g = 2.18$  and  $D_{\text{ion}} = 2.07 \text{ cm}^{-1}$  for **1RR** ( $R = 8.1 \cdot 10^{-6}$ )  $J = +19.2 \text{ cm}^{-1}$ ,  $g = 2.23$  and  $D_{\text{ion}} = 2.30 \text{ cm}^{-1}$  for **2RR** ( $R = 1.8 \cdot 10^{-5}$ ). From these  $J$  values it can be inferred that the ground state is a well isolated  $S = 2$  level. The magnetization data show a quasi saturated values of  $4.32$  and  $4.24 \text{ N}\mu_B$  for **1RR** and **2RR** respectively. These results show good agreement with the expected magnetic response and the reported values for  $[\text{Ni}_2(\text{L}5)(\text{N}_3)_2](\text{ClO}_4)_2$  and  $[\text{Ni}_2(\text{L}5)(\text{N}_3)_2](\text{ClO}_4)_2$ .<sup>[40]</sup>

### Conclusions

A complete family of  $\text{Ni}^{\text{II}}$  dimers built from bis-bidentate Schiff bases with the general formula  $[\text{Ni}_2(\text{L})_2(\text{N}_3)_2]^{2+}$ , showing the transition from mesocate to helicite conformation, has been structurally characterized and related to the flexibility of the central spacer of the ligands and the size of the substituents of the Schiff base (pyridyl/quinoxalyl). The ECD spectra in solid state and solution have been measured for two pairs of enantiomers showing that the systems are stable in solution and their spectra have been rationalized by DFT calculations. It is remarkable the unprecedented structure of complex **7** that shows the simultaneous crystallization of both conformations in

the same unit cell and the characterization of the first coordination compound derived of the imine-quinoxalyl ligand L4.

## Experimental Section

**Physical measurements:** Magnetic susceptibility measurements were carried out on polycrystalline samples with a MPMS5 Quantum Design susceptometer working in the range 30–300 K under magnetic fields of 0.3 T and under a field of 0.03T in the 30 – 2 K range to avoid saturation effects at low temperature. Diamagnetic corrections were estimated from Pascal Tables. Infrared spectra ( $4000\text{--}400\text{ cm}^{-1}$ ) were recorded from KBr pellets on a Bruker IFS-125 FT-IR spectrophotometer. ECD spectra were recorded with a Jasco J-710 spectropolarimeter. Solution spectra were recorded in  $2 \cdot 10^{-4}$  M  $\text{CH}_3\text{CN}$  solutions; solid state spectra were recorded using the KCl pellet technique. In order to rule out the occurrence of contributions from linear dichroism/linear birefringence due to preferential orientation of the solid sample, the disc was rotated by  $90^\circ$ ,  $180^\circ$ ,  $270^\circ$  and then flipped around its  $C_2$  axis. A spectrum was recorded after each rotation to check that no significant difference depending on the rotation angle was present. VCD spectra were recorded with a Jasco FVS 6000 spectropolarimeter on KCl discs.

**DFT calculations:** Calculations were run with Gaussian09, rev. D01,<sup>[57]</sup> starting from the X-ray geometry of **1SS** which was fully re-optimized at B3LYP/6-31G(d) level to a true energy minimum (no imaginary frequencies). A structure with +2 charge and quintet spin state was used in all calculations. Excited states TDDFT calculations were run with several different functionals, including B3LYP, CAM-B3LYP, X3LYP, BH&HLYP, PBE-1/3, and basis sets, including SVP, TZVP and LanL2DZ (with ECP for Ni), including up to 100 excited states (roots).

**Single-crystal X-ray structure analyses:** Prism-like specimens of **1M**, **1SS**, **1RR**, **2SS**, **2RR**, **4R** and **7** and multiple crystals of the complexes derived from L3 were used for the X-ray crystallographic analysis. The X-ray intensity data were measured on a D8-Venture system equipped with a multilayer monochromator and a Mo microfocus ( $\lambda = 0.71073\text{ \AA}$ ). The frames were integrated with the Bruker SAINT software package using a narrow-frame algorithm. The final cell constants were based upon the refinement of the XYZ-centroids of reflections above  $20\sigma(I)$ . Data were corrected for absorption effects using the multi-scan method (SADABS). The structures were solved using the Bruker SHELXTL Software Package, and refined using SHELXL.<sup>[58]</sup> Details of crystal data, collection and refinement are summarized in Tables S6–S9. Analyses of the structures and plots for publication were performed with Ortep3<sup>[59]</sup> and POVray programs.

### Syntheses.

Schiff bases L1 and L2 were isolated as solids whereas L3, L4 and L7 were prepared *in situ* and the ligand solution was employed directly to synthesize the corresponding complexes.

**Rac-L1**, **RR-L1** and **SS-L1**: syntheses were common for the racemic or enantiomerically pure ligands **Rac-L1**, **RR-L1** and **SS-L1**. A solution of 2-pyridinecarboxaldehyde (3.9 mmol) and the corresponding diaminocyclohexane isomer (1.75 mmol) in 20 mL of methanol was stirred for 2 hours at room temperature. Concentration *in vacuo* afforded ligands L1 as white solids that were recrystallized in diethyl ether.

**RR-L2** and **SS-L2**: A similar procedure was employed for **RR-L2** and **SS-L2**. A solution of the corresponding isomer of 1,2-cyclohexanediamine

(0.5 mmol) and 2-quinolinecarboxaldehyde (1 mmol) were mixed in 20 mL of dichloromethane and stirred at room temperature for 24 hours. After concentration at one half of the volume, the solution was mixed with 20 mL of *n*-hexane. L2 was collected as a yellowish powder. Recrystallization in diethyl ether afforded the yellowish crystals used for the syntheses. IR spectra are shown in Figure S4.

**$[\text{Ni}_2(\text{L})_2(\text{N}_3)_2](\text{NO}_3)_2 \cdot n\text{MeOH}$  (L = L1, **1M-2MeOH**, **1RR-2MeOH**, **1SS-2MeOH**; L = L2, **2RR-3MeOH**, **2SS-3MeOH**).** The complexes were synthesized following the same experimental procedure: 1 mmol of the corresponding L1 or L2 ligand and 1 mmol of  $\text{Ni}(\text{NO}_3)_2 \cdot 6\text{H}_2\text{O}$  were solved in 20 mL of methanol and stirred for some minutes. To this solution was added 1 mmol of sodium azide solved in 5 mL of methanol. Crystallization by vapor diffusion of diethylether afforded well formed reddish crystals after one-two days. Anal. Calc/found (%) for **1M/1RR/1SS** as  $\text{C}_{38}\text{H}_{48}\text{N}_{16}\text{Ni}_2\text{O}_8$ : C, 46.85/46.8/46.4/46.5; N, 23.00/22.9/23.2/23.4; H, 4.97/4.6/4.3/5.1. Calc/found (%) for **2RR/2SS** as  $\text{C}_{55}\text{H}_{60}\text{N}_{16}\text{Ni}_2\text{O}_9$ : C, 54.75/53.9/54.3/54.2; N, 18.57/18.9/18.3/18.5; H, 5.01/4.8/4.7/5.2. IR spectra are shown in Figure S4.

**$[\text{Ni}_2(\text{R-L4})_2(\text{N}_3)_2](\text{ClO}_4)_2 \cdot \text{H}_2\text{O}$  (**4R-0.25H<sub>2</sub>O**),** were synthesized by preparing the ligand *in situ* by mixing 0.25 mmols of *R*- or *S*-1,2-diaminopropane hydrochloride with 0.5 of triethylamine and 0.5 mmols of quinoline carboxaldehyde. The mixture was refluxed in MeOH for 1h. After cooling down were added to the mixture 0.25 mmols of  $\text{Ni}(\text{ClO}_4)_2 \cdot 6\text{H}_2\text{O}$  and 0.25 mmols of  $\text{NaN}_3$ . The mixture was stirred at room temperature 30 more minutes and filtered. Crystallization by vapour diffusion of diethylether produced well formed reddish crystals after few days. Anal. Calc/found (%) for **4R** as  $\text{C}_{46}\text{H}_{40.5}\text{Cl}_2\text{N}_{14}\text{Ni}_2\text{O}_{8.25}$ : C, 49.79/49.3; N, 17.67/17.4; H, 3.67/3.8. IR spectra are shown in Figure S5.

**$[\text{Ni}_2(\text{L3})_2(\text{N}_3)_2](\text{X})_2$  (**3**) (X =  $\text{NO}_3^-$ ,  $\text{ClO}_4^-$ ).** The six complexes derived from L3 (meso, *R* and *S*) were synthesized in the search of adequate crystals to obtain structural information, but all data collection were unsuccessful. The syntheses were performed following the same procedure employed for **4R**. IR spectra are shown in Figure S6.

**$[\text{Ni}_2(\text{L7})_2(\text{N}_3)_2](\text{NO}_3)_2 \cdot 2\text{H}_2\text{O} \cdot 2\text{MeOH}$  (**7-2H<sub>2</sub>O-2MeOH**)** was prepared synthesizing the ligand *in situ* by mixing 0.025 mmols of ethylenediamine and 0.5 mmols of quinoline carboxaldehyde and refluxing during 1h. After cooling down, to the mixture were added 0.25 mmols of  $\text{Ni}(\text{NO}_3)_2 \cdot 6\text{H}_2\text{O}$  and 0.25 mmols of sodium azide and stirred at room temperature 30 minutes. The solution was filtered and layered with diethylether. Red crystals were obtained after a few days. Anal. Calc/found (%) for **7** as  $\text{C}_{67}\text{H}_{61}\text{N}_{24}\text{Ni}_2\text{O}_{11}$ : C, 51.77/51.5; N, 21.63/21.8; H, 3.96/3.8. IR spectrum is shown in Figure S5.

## Acknowledgements

JM and AE thanks financial support from Ministerio de Economía y Competitividad, Project CTQ2015-63614-P.

**Keywords:** helicate • mesocate • chirality • nickel • Circular dichroism

- [1] O. Mamula, A. von Zelewsky, *Coord. Chem. Rev.* **2003**, *242*, 87–95.
- [2] D. Amabilino in *Chirality at the Nanoscale, Nanoparticles, Surfaces, Materials and more*. Wiley-VCH, **2009**.
- [3] A. Myari, N. Hadjiliadis, A. Garoufis, *J. Inorg. Biochem.* **2005**, *99*, 616–626.

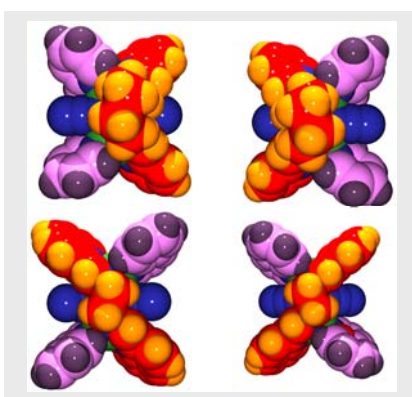
- [4] E. Francotte, W. Lindner in *Chirality in the Drug Research*. Wiley-VCH, Weinheim, **2006**.
- [5] K. Szacilowski, W. Mazyk, A. Drzewiecka-Matuszek, M. Brindell, G. Stochel, *Chem. Rev.* **2005**, *105*, 2647-2694.
- [6] E. Yashima, N. Ousaka†, D. Taura, K. Shimomura, T. Ikai, K. Maeda, *Chem. Rev.* **2016**, 13752-13990.
- [7] Y. Inoue, V. Ramamurthy in *Chiral Photochemistry*; Marcel Dekker; New York, **2004**, pp. 261-313.
- [8] K. Mikami, M. Lentens in *New Frontiers in Asymmetric Catalysis*. Wiley-VCH, **2007**.
- [9] R. Gomez, J. Adrio, J. C. Carretero, *Angew. Chem. Int. Ed.* **2006**, *45*, 7674-7715.
- [10] G. C. Fu, *Acc. Chem. Res.* **2006**, *39*, 853-860.
- [11] T. Katsuki, *Chem. Soc. Rev.* **2004**, 437-444.
- [12] G. Chelucci, R. P. Thummel, *Chem. Rev.* **2002**, *102*, 3129-3170.
- [13] J. M. Lehn in *Supramolecular Chemistry: Concepts and Perspectives*. VCH, Weinheim, **1995**.
- [14] J. W. Steel, J. L. Atwood in *Supramolecular Chemistry* Wiley ed., Chippinham, **2009**.
- [15] M. Albrecht, *Chem.-A Eur J.* **2000**, *6*, 3485-3489.
- [16] B. W. Ding, R. Keese, H. Stoeckli-Evans, *Angew. Chem. Int. Ed.* **1999**, *38*, 375-376.
- [17] J. Xu, K. N. Raymond, *Angew. Chem. Int. Ed.* **2006**, *45*, 6480-6485.
- [18] M. A. Masood, E. J. Enemark, T. D. P. Stack, *Angew. Chem. Int. Ed.* **1998**, *37*, 928-932.
- [19] V. Amendola, L. Fabbrizzi, L. Linati, C. Mangano, P. Pallavicini, V. Pedrazzini, M. Zema, *Chem. Eur. J.* **1999**, *5*, 3679-3688.
- [20] V. Amendola, L. Fabbrizzi, C. Mangano, P. Pallavicini, E. Roboli, M. Zema, *Inorg. Chem.* **2000**, *39*, 5803-5806.
- [21] P. K. Pal, S. Chowdhury, P. Purkayastha, D. A. Tocher, D. Datta, *Inorg. Chem. Commun.* **2000**, *3*, 585-589.
- [22] V. Amendola, L. Fabbrizzi, L. Gianelli, C. Maggi, C. Mangano, P. Pallavicini, M. Zema, *Inorg. Chem.* **2001**, *40*, 3579-3587.
- [23] R. Zissel, P. Nguyen, L. Douce, M. Cesario, C. Estournes, *Org. Lett.* **2004**, *6*, 2865-2868.
- [24] G. K. Patra, I. Goldberg, *New J. Chem.* **2003**, *27*, 1124-1131.
- [25] N. C. Habermehl, P. M. Angus, N. L. Kilah, L. Noren, A. D. Rae, A. C. Willis, S. B. Wild, *Inorg. Chem.* **2006**, *45*, 1445-1462.
- [26] A. Ouali, M. Taillefer, J. F. Spindler, A. Jutand, *Organometallics* **2007**, *26*, 65-74.
- [27] P. Pallavicini, M. Boiocchi, G. Dacarro, C. Mangano, *New J. Chem.* **2007**, *31*, 927-935.
- [28] V. Amendola, M. Boiocchi, V. Brega, L. Fabbrizzi, L. Mosca, *Inorg. Chem.* **2010**, *49*, 997-1007.
- [29] M. Boiocchi, V. Brega, C. Ciarrocchi, L. Fabbrizzi, P. Pallavicini, *Inorg. Chem.* **2013**, *52*, 10643-10652.
- [30] van Stein, G. C.; van Koten, G.; Vrieze, K.; Brevard, C.; Spek, A. L. *Chem. Commun.* **1980**, 1016-1018.
- [31] van Stein, G. C.; van Koten, G.; Vrieze, K.; Brevard, C.; Spek, A. L. *J. Am. Chem. Soc.* **1984**, *106*, 4486-4492.
- [32] Bowyer, P. K.; Porter, K. A.; Rae, A. D.; Willis, A. C.; Wild, S. B. *Chem. Commun.* **1998**, 1153-1154.
- [33] Amendola, V.; Fernandez, Y. D.; Mangano, C.; Montalti, M.; Pallavicini, P.; Prodi, L.; Zaccheroni, N.; Zema, M. *Dalton Trans.* **2003**, 4340-4345.
- [34] Khalaji, A. D.; Amirasr, M.; Welter, R. *Anal. Sci.: X-Ray Struct. Anal. Online* **2006**, *22*, x151-x152.
- [35] Constable, E. C.; Zhang, G.; Housecroft, C. E.; Zampese, J. A. *CrystEngComm* **2010**, *12*, 3724-3732.
- [36] E. C. Constable, G. Zhang, C. E. Housecroft, M. Neuburger, J. A. Zampese, *Eur. J. Inorg. Chem.* **2010**, 2000-2011.
- [37] E. C. Constable, G. Zhang, C. E. Housecroft, J. A. Zampese, *Dalton Trans.* **2010**, 5332-5340.
- [38] T. Takeda, S. Harada, A. Nishida *Org. Lett.* **2015**, *17*, 5184-5187.
- [39] Y. I. Cho, D. M. Joseph, M. J. Rose, *Inorg. Chem.* **2013**, *52*, 13298-13300.
- [40] M. Habib, T. K. Karmakar, G. Aromi, J. Ribas-Arino, H.-K. Fun, S. Chantrapromma, S. K. Chandra, *Inorg. Chem.* **2008**, *47*, 4109-4117.
- [41] J. Crassous, *Chem. Soc. Rev.* **2009**, *38*, 830-845.
- [42] M. Liu, L. Zhang, T. Wang, *Chem. Rev.* **2015**, *115*, 7304-7397.
- [43] A. Frontera, P. Gamez, M. Mascal, T. J. Mooibroek, J. Reedijk, *Angew. Chem. Int. Ed.* **2011**, *50*, 9564-9583.
- [44] M. Nishio, *CrystEngComm.* **2004**, *6*, 130-158.
- [45] R. Berardozi, E. Badetti, N. A. Carmo dos Santos, K. Wurst, G. Licini, G. Pescitelli, C. Zonta, L. Di Bari, *Chem. Commun.* **2016**, *52*, 8428-8431.
- [46] S. R. Domingos, H. J. Sanders, F. Hartl, W. J. Buma, S. Woutersen, *Angew. Chem. Int. Ed.* **2014**, *53*, 14042-14045.
- [47] L. A. Nafie, *J. Phys. Chem. A* **2004**, *108*, 7222-7231.
- [48] G. Pescitelli, T. Kurtán, U. Flörke, K. Krohn, *Chirality* **2009**, *21*, E181-E201.
- [49] D. Padula, S. Di Pietro, M. A. M. Capozzi, C. Cardellicchio, G. Pescitelli, *Chirality* **2014**, *26*, 462-470.
- [50] M. Srebro-Hooper, J. Autschbach, *Annu. Rev. Phys. Chem.* **2017**, *68*, 399-420.
- [51] A. Ipatov, F. Cordova, L. J. Doriol, M. E. Casida, *J. Mol. Struct.: THEOCHEM* **2009**, *914*, 60-73.
- [52] M. Enamullah, M. A. Qudus, M. R. Hasan, G. Pescitelli, R. Berardozi, G. Makhloufi, V. Vasylyeva, C. Janiak, *Dalton Trans.* **2016**, *45*, 667-680.
- [53] M. E. Casida, C. Jamorski, K. C. Casida, D. R. Salahub, *The Journal of Chemical Physics* **1998**, *108*, 4439-4449.
- [54] A. Lützen, M. Hapke, J. Griep-Raming, D. Haase, W. Saak, *Angew. Chem. Int. Ed.* **2002**, *41*, 2086-2089.
- [55] A. Escuer, J. Esteban, S. P. Perlepes, T. C. Stamatatos, *Coord. Chem. Rev.* **2014**, *275*, 87-129.
- [56] N. F. Chilton, R. P. Anderson, L. D. Turner, A. Soncini, K. S. Murray, *J. Comput. Chem.* **2013**, *34*, 1164-1165.
- [57] M. J. Frisch, G. W. Trucks, H. B. Schlegel, G. E. Scuseria, M. A. Robb, J. R. Cheeseman, G. Scalmani, V. Barone, B. Mennucci, G. A. Petersson, H. Nakatsuji, M. Caricato, X. Li, H. P. Hratchian, A. F. Izmaylov, J. Bloino, G. Zheng, J. L. Sonnenberg, M. Hada, M. Ehara, K. Toyota, R. Fukuda, J. Hasegawa, M. Ishida, T. Nakajima, Y. Honda, O. Kitao, H. Nakai, T. Vreven, J. J. A. Montgomery, J. E. Peralta, F. Ogliaro, M. Bearpark, J. J. Heyd, E. Brothers, K. N. Kudin, V. N. Staroverov, R. Kobayashi, J. Normand, K. Raghavachari, A. Rendell, J. C. Burant, S. S. Iyengar, J. Tomasi, M. Cossi, N. Rega, J. M. Millam, M. Klene, J. E. Knox, J. B. Cross, V. Bakken, C. Adamo, J. Jaramillo, R. Gomperts, R. E. Stratmann, O. Yazyev, A. J. Austin, R. Cammi, C. Pomelli, J. W. Ochterski, R. L. Martin, K. Morokuma, V. G. Zakrzewski, G. A. Voth, P. Salvador, J. J. Dannenberg, S. Dapprich, A. D. Daniels, O. Farkas, J. B. Foresman, J. V. Ortiz, J. Cioslowski, D. J. Fox, Gaussian 09, Revision D.01, Gaussian, Inc.: Wallingford CT, 2013.
- [58] G. M. Sheldrick, *Acta Crystallogr. Sect A: Fundam. Crystallogr.* **2008**, *64*, 112-122.
- [59] L. J. Farrugia, *J. Appl. Crystallogr.* **1997**, *30*, 565.

**Entry for the Table of Contents**

Layout 1:

**FULL PAPER**

The transition from mesocate to helicate conformations in a series of dinuclear nickel(II) complexes has been reached tailoring the flexibility and size of the ligands. Chiral mesocates have been achieved.



Júlia Mayans, Mercè Font-Bardia,  
Lorenzo Di Bari, Lorenzo Arrico,  
Francesco Zinna, Gennaro Pescitelli,  
Albert Escuer\*

*Page No. – Page No.*

**From Mesocates to Helicates:  
Nickel(II) Supramolecular Assemblies  
Derived from Tetradentate Schiff  
Bases. Structural, Magnetic and  
Chiro-Optical Studies.**